Journal of Nuclear Materials 403 (2010) 75–88

Contents lists available at ScienceDirect

Journal of Nuclear Materials

journal homepage: www.elsevier.com/locate/jnucmat

Microstructural evolution of irradiated tungsten: *Ab initio* parameterisation of an OKMC model

C.S. Becquart [a,*], C. Domain [a,b], U. Sarkar [a,c], A. DeBacker [a], M. Hou [d]

[a] *Unité Matériaux et Transformations, UMR 8207, Université de Lille 1, F-59655 Villeneuve d'Ascq Cedex, France*
[b] *EDF-R&D Département MMC, Les Renardières, F-77818 Moret sur Loing Cedex, France*
[c] *Physics Department, Assam University, Silchar, India*
[d] *Physique des Solides Irradiés et des Nanostructures CP234, Université Libre de Bruxelles, Bd du Triomphe, B-1050 Brussels, Belgium*

ARTICLE INFO

Article history:
Received 5 March 2010
Accepted 1 June 2010

ABSTRACT

It is important to develop an understanding of the evolution of W microstructure under the conditions expected in the International Thermonuclear Experimental Reactor as well as the DEMOnstration Power Plant, Modelling techniques can be very helpful in this regards. In this paper, an object kinetic Monte Carlo code has been parameterised on *ab initio* calculations to model the behaviour of helium atoms implanted in tungsten, in the presence or not of the point defects created during the implantation. The slowing down of atomic helium in tungsten as well as the associated Frenkel Pair production is determined using the Marlowe code and is described in a paper companion to this one. The OKMC simulations indicate that He desorption results from a competition between the formation of mobile clusters and sessile ones, and it is thus very important to model correctly their spatial distributions as well as their properties.

1. Introduction

Producing electricity using nuclear fusion implies a good knowledge of materials behaviour under the simultaneous assault of a plasma, fluxes of Helium and Hydrogen isotopes (deuterium and tritium) as well as the 14 MeV neutrons produced during the fusion reaction. In the International Thermonuclear Experimental Reactor (ITER), tungsten is considered for the divertor, one part of the reactor which will face the plasma at temperatures in the range of 1273 K. Its use in the DEMOnstration Power Plant (DEMO), the reactor which will have to be built to validate this new means of electricity production, implies to be able to predict the behaviour of this materials in even more extreme conditions in DEMO, the amount of 14 MeV neutrons produced will be much larger than in ITER, as DEMO should be four times more powerful.

In principle, the object kinetic Monte Carlo (OKMC) method can be used to model the microstructure evolution of materials under such conditions, covering from the atomic to the mesoscopic scales. However, it requires, for the microstructure to be modelled, the knowledge of interaction mechanisms between objects such as point defects and their clusters, solute elements, and dislocations. The elementary physical phenomena associated with the point defects created and their interaction with the different elements of the microstructure have thus to be determined. Their integration into a coherent model requires atomic level information. Part of it are provided by experiment. Other parts, such as the stability and migration properties of point defects, and small clusters may be obtained by means of *ab initio* calculations. In this article we describe the strategy followed to parameterise an OKMC model aiming at simulating radiation damage in tungsten in the presence of He. As no valid interatomic potential for the W–He system is available at the moment, allowing a classical molecular dynamics (MD) approach, this parameterisation relies on a large number of *ab initio* calculations as well as on a set of isochronal annealing experiments of He desorption in W. The slowing down of helium atoms is determined using the Binary Collision Approximation (BCA) and is described in a companion paper to this one [1]. The first part of the paper briefly presents the OKMC model. The second part is devoted to the parameterisation of the model. After a brief review of the interatomic potentials available at the moment and their shortcomings, the strategy followed for the parameterisation in this work is presented, first for the case where only He atoms are introduced in the matrix (under-threshold He implantations), then for above-threshold He implantations, i.e. in the presence of point defects and their clusters.

2. Methodology

2.1. The object kinetic Monte Carlo code

The OKMC code LAKIMOCA developed at EDF has been extended to take into account Foreign Interstitial Atoms (FIAs – He in the present work).

* Corresponding author. Tel.: +33 3 20 43 49 44; fax: +33 3 20 33 61 48.
E-mail address: charlotte.becquart@univ-lille1.fr (C.S. Becquart).

0022-3115/$ - see front matter © 2010 Elsevier B.V. All rights reserved.
doi:10.1016/j.jnucmat.2010.06.003

The general features of the LAKIMOCA code, nowadays available, have been extensively described in a previous publication [2]. Further developments concern the treatment of Foreign Interstitial Atoms (FIAs) and their features. In brief, the model treats radiation produced defects (vacancies, self-interstitial atoms (SIA) and their clusters) as well as FIAs as objects with specific positions in a simulation box and with associated reaction volumes. The objects include vacancy and SIA clusters of all sizes as well as clusters of mixed type (vacancy–FIA and SIA-FIA objects). Depending on its nature, each object can migrate and participate in a series of predefined reactions. It can emit single entities, a vacancy, a SIA or a FIA, if the object contains this entity. Within this scheme, the emission of one or more than one SIA and vacancies from a pure FIA cluster which has been observed in Mo for instance [3] is not allowed. The object properties are: the types of objects (for example, a single vacancy v, a He atom, a di-vacancy, 2v, a single self-interstitial atom (SIA), etc.), the forward reactions that these objects can perform with the appropriate probabilities and capture radii (for example, the annihilation of a vacancy with a self-interstitial: $v + SIA \rightarrow \varnothing$, or the formation of a di-vacancy: $v + v \rightarrow 2v$), the backward reactions with their probabilities (for example, the dissociation of a vacancy from a di-vacancy). The probabilities for physical transition mechanisms Γ_i, which are basically migration jumps and emission from larger defects or from traps, are calculated in terms of Arrhenius frequencies for thermally activated events,

$$\Gamma_i = \nu_i \exp\left(\frac{-E_{a,i}}{k_B T}\right) \tag{1}$$

where ν_i is the attempt frequency (prefactor) for event i, $E_{a,i}$ is the corresponding activation energy, k_B is Boltzmann's constant and T is the absolute temperature.

For an object to migrate, $E_{a,i}$ is the migration energy of the object; for an object to emit a single entity x, $E_{a,i}$ is the dissociation energy, i.e. the sum of the binding energy of x with the object plus its migration energy.

Time evolves according to the residence time algorithm [4,5].

$$\Delta\tau = 1 \Big/ \sum_{i=1}^{N_e^{th}} \Gamma_i + \sum_{j=1}^{N_e^{ext}} P_j \tag{2}$$

where P_j are the probabilities of external events, such as the appearance of a cascade, of isolated Frenkel pairs produced by impinging particles, or implanted FIAs. In addition, the model includes non-thermally activated events, such as the annihilation of a defect after encountering either a defect of opposite nature (i.e. a SIA encountering a vacancy) or a sink, as well aggregation, either by adding a point defect to a cluster or by forming a complex between a defect and a trap. These events occur only on the basis of geometrical considerations (overlap of reaction volumes) and do not participate in defining the progressing of time. Trapping and annihilation of defects with opposite defects or at sinks, as well as aggregation into larger clusters, take place spontaneously whenever the involved objects come to a mutual distance smaller than a reaction distance, which is equal to the sum of the capture radii associated to each of the two objects, as explained in the description of the parameter sets. The capture radius depends on the object type, size and shape. The possibility of introducing different classes of immobile traps and sinks, characterised by specific geometrical shapes (spheres, infinite cylinders, surfaces, ...) and suitable to mimic voids or other trapping nano-features, as well as dislocations and grain boundaries, is also implemented. The code is therefore equipped to mimic fairly realistic microstructures and irradiation conditions. Fig. 1 summarises the different objects and events which can take place in the simulation box.

Besides introducing appropriate reactions in the model, their parameterisation is another very difficult task. To each possible motion corresponds a migration energy and an attempt frequency. One thus needs to know the migration energies (and attempt frequencies) of all the possible objects that are believed to form, move and interact in the course of the simulation. Because of the Arrhenius dependence of Eq. (1), one usually concentrates its effort on the determination of the migration energies, i.e. the energy barrier the moving species have to overcome to migrate, and the attempt frequencies are taken to be as constants of the order of the Debye frequency. The same reasoning is applied to the dissociation events and the efforts are, there, concentrated on the binding energies. The binding energy between A and B, where A is for instance a cluster containing $(n-1)$ He atoms and B is a single He atom, is the difference in energy between two systems: one system where the two elements are far from each other and do not interact; and the same system, but where A and B interact, i.e. form a cluster containing nHe atoms. In our scheme, a positive binding energy indicates attraction between A and B, i.e. in the example proposed here, a positive binding energy indicates that

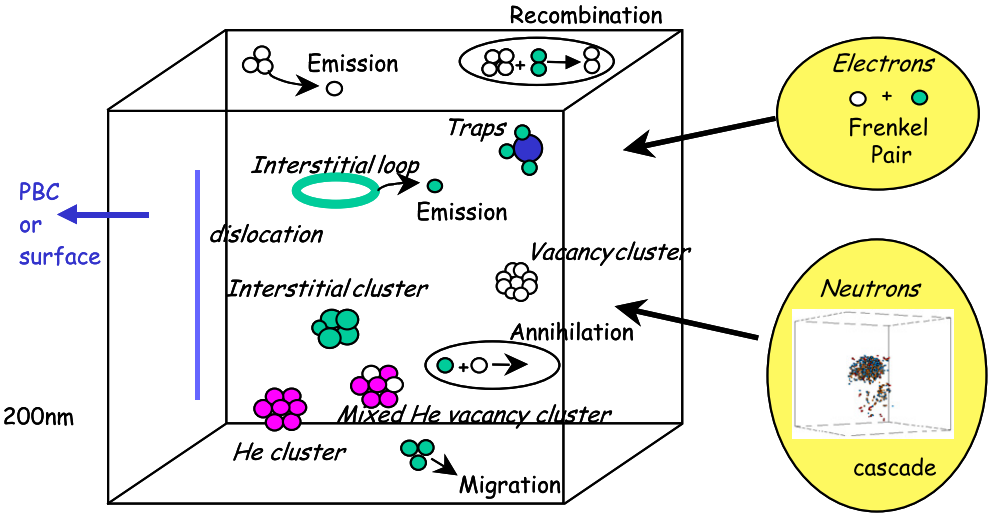

Fig. 1. Summary of the different events: migration, recombination, emission of single entities or trapping as well as electron or neutron irradiations, taking place in an object KMC simulation using the LAKIMOCA code. The white spheres are the vacancies, the green ones, the SIAs; the pink ones represent the helium atoms. (For interpretation of the references to colour in this figure legend, the reader is referred to the web version of this article.)

an He atom will prefer to be in a cluster containing *n*He atom rather than isolated.

As very few data exist in the literature about binding and migration energies of the elements modelled in the OKMC code, one has to turn to simulation results to obtain these data. One approach would consist in using MD simulations; however, as will be shown in the next sections, no W–He potential is currently available that correctly reproduces the basic properties of the point defects and He atoms.

2.2. Assessment of the empirical potentials available

To obtain the distribution of the He atoms implanted as well as the associated primary damage, the most appropriate tool is Molecular Dynamics, which relies on the use of empirical potentials. Furthermore, as stated in the introduction, data related to the behaviour of defect clusters cannot be obtained using *ab initio* calculations when the clusters are big, as *ab initio* calculations are limited by the size of the supercells which can be currently modelled. Reliable interatomic potentials are thus necessary and we briefly review in the next paragraph the potentials available at the moment to model tungsten and He in tungsten.

Many empirical potentials have been derived for body-centred cubic (bcc) metals, and for tungsten in particular. In 1972, Johnson and Wilson [6] developed central potentials to calculate vacancy migration energies and di-vacancy binding energies as well as phonon dispersion curves in bcc metals. In 1978, Johnson and White [7] proposed a modified W–W which increased previously reported surface energies in W by about 9%. In 1983, Johnson [8] derived two other potentials dedicated to the study of interstitials. In 1984, Finnis and Sinclair [9] proposed a simple empirical N-body potential for transition metals, which was later used by Harder and Bacon [10] to study point defect and stacking fault properties in body-centred-cubic metals, and by Ackland and Finnis [11] to evaluated solid surface tensions in body-centred cubic transition metals. In 1987, Ackland and Thetford [12] derived an improved N-body semi-empirical model for body-centred cubic transition metals which was used by Harder and Bacon [13] to investigate the structure of small interstitial clusters in bcc metals. In 1989, Johnson and Oh [14], proposed an analytical embedded atom method model for bcc metals. Other analytical EAM interatomic potentials for bcc transition metals were constructed to study point-defect properties in bcc transition metals by Hu and collaborators [15]. Because the bonding in transition metals has a mixed nearly free electron and covalent character, some attempts were made to build non-central interatomic interactions as for instance in [16] where Carlsson introduced angular components in the formulation of interatomic potentials for bcc transition metals in an attempt to better describe structural energy differences, or in [17] by Baskes who proposed his modified embedded atom method (MEAM) for cubic materials and impurities or in [18] where Lee and co-workers developed a second nearest neighbour modified embedded atom method potentials for bcc transition metals. With the advances in solid state theory and in particular in the understanding of bonding, more and more care was taken to introduce first principle "ingredients" in deriving the potentials. In 1993, Foiles [19] derived interatomic interactions for Mo and W based on the low-order moments of the density of states which improve the description of environments that deviate from the bulk bcc metal, i.e. dislocation core structures and grain boundaries. In 1994, Xu and Adams, [20] used Carlsson's approach of the low-order moments approximation to tight binding, to develop improved potentials for Mo and W. In 1995, Wang and Boercker [21] derived an effective interatomic potential suitable for all bcc metals based on the EAM. In 1997, Xie and Chen [22] developed semi-empirical tight-binding interatomic potentials based on the Hubbard model. In 2001, Mundim and co-workers [23] investigated the diffusion properties of tungsten using an interatomic potential which had been extracted with a recursive procedure from *ab initio* calculations (using the Linear Muffin Tin Orbitals method in the Atomic Sphere Approximation (LMTO-ASA)) of the cohesive energy. Recently, Juslin and co-workers [24] developed a reactive interatomic potential based on an analytical bond order scheme for the ternary system W–H–C. Even more recently, two new potentials were derived for tungsten: a Finnis–Sinclair type based on *ab initio* data [25] as well as a Bond Order Potential (BOP) one fitted on Tight Binding Linear Muffin Tin Orbital (TB-LMTO) calculations [26].

There seems thus to be many interatomic potentials available for tungsten, however, for our purpose, it is important that the potentials reproduce correctly the basic point-defect properties which we now examine.

2.2.1. SIA properties

In bcc metals, the SIAs are dumbbells, i.e. two atoms sharing one crystallographic sites. The relative stability of the possible dumbbells ($\langle 1\,0\,0\rangle$, $\langle 1\,1\,0\rangle$ or $\langle 1\,1\,1\rangle$ dumbbells) has proven to be significant in predicting the SIA migration behaviour in Fe and as a result the prediction of the primary damage [27,28]. Most experimental results [29–31] as well as MD simulations using "old" potentials (Guinan et al. [32] using the potential derived by Johnson in 1972 [6]; and Carlberg et al. [33] using the potential also derived by Johnson but in 1989 [14]) seem to indicate that in W the $\langle 1\,1\,0\rangle$ dumbbell is the most stable SIA configuration. However, *ab initio* calculations using PLATO [34] and VASP [35] have showed that it is the $\langle 1\,1\,1\rangle$dumbbell which is the most stable. These calculations are quite tricky because of the strain field induced by the SIA and they need to be performed with large supercells. Indeed, our *ab initio* calculations lead to an energy difference between the $\langle 1\,1\,0\rangle$ and the $\langle 1\,1\,1\rangle$ dumbbell, $\Delta E_{\langle 111\rangle-\langle 110\rangle}$, very close to 0 eV for a 54 atom supercell, (the $\langle 1\,1\,1\rangle$ dumbbell being slightly more stable), 0.26 eV for a 128 atom supercell and 0.28 eV for a 250 atom supercell. The recent potential derived by Derlet et al. [25], which was adjusted on *ab initio* data predicts the $\langle 1\,1\,1\rangle$ dumbbell to be the most stable and appears thus suitable from this point of view. Finally, the equally recent BOP potential derived by Mrovec et al. [26], is unsuitable for simulations of atomic configurations where the short-range repulsion is dominant, i.e. self-interstitials and interstitial impurities according to its authors.

Predicting the correct stability of the SIA may not have too much influence for our modelling, however, its migration energy is a crucial quantity in the modelling of radiation damage. The experimental migration energies are usually obtained from isochronal annealing experiments. In these kinds of experiments, the materials are first irradiated at very low temperatures. Generally, the irradiating particles are electrons and the damage created is in the form of isolated FPs. The irradiated materials are then isochronally annealed at a specific rate and their recovery is analysed either by electrical resistivity, magnetic after-effect or internal friction measurements. The differential isochronal resistivity recovery spectra exhibit a certain number of peaks which can be associated with several processes involving the different point defects and their clusters. The events taking place at low temperatures (below 200 K) are usually associated with events involving only SIA-type defects and their clusters (the SIA migration energy in metals is always much lower than the vacancy migration energy).

For tungsten, the situation is a bit complicated as stage I of the isochronal annealing resistivity recovery of irradiated tungsten, is composed of many peaks: eight intrinsic recovery stages are mentioned by Dausinger [36], one large peak and six smaller ones by Di Carlo et al. [30] while five sub-stages were observed by Coltman et al. [37] and Maury and co-workers [38]. These peaks evolve or

not with dose or with the amount of impurities and the migration energy deduced by the different authors spans from 0.08 eV [39] to 0.054 eV [40]. More recently, Tanimoto [41] even proposed that the SIA is mobile below 1.5 K which would imply that its migration energy is close to 0.

Simulations based on the "old" interatomic potentials predict much higher values than the ones obtained from the isochronal annealing experiments. MD simulations based on the potentials developed by Johnson lead to a migration barrier for the ⟨1 1 0⟩ SIA of 0.37 eV [32] or 0.54 eV [33]. This problem is solved with the potential derived by Derlet [25] which predicts that the SIA indeed moves very quickly, with a migration energy of 0.013 eV. Furthermore, the SIA being a ⟨1 1 1⟩ crowdion it moves along ⟨1 1 1⟩ directions in a 1D type motion. Note that SIA clusters were found to be also very mobile [42] with this potential. Note that as indicated in [43] care has to be taken when determining the SIA migration energies as static calculations may not give the same results as dynamic ones.

2.2.2. Vacancy properties

The experimental data for the vacancy formation energy are quite scattered as it lies between 3.1 eV [44] and 4.0 eV [44,45]. Indeed self diffusion in many bcc metals is still an open question at high temperatures, where two-defect models [46] compete with one-defect models [47]. Depending on the model one chooses to apply, as well as the experimental dataset, the activation energy for self diffusion, *Q*, varies (for the first defect) between 5.2 eV (6.62 eV for the 2nd defect) and 5.62 eV (7.33 eV for the 2nd defect) [46] if one assumes a two-defect model, or between 6.08 eV and 6.6 eV [47] if one assumes a one defect model. The type of the two defects in the two-defect model (mono-vacancies, di-vacancies, interstitials) is still very much debated. In the lower temperature range, however, there is no question that mono-vacancies dominate the diffusivity. However despite such a large range of experimental data, some of the potentials derived more recently appear to misreproduce this value. The values obtained by the two potentials derived by Carlsson [16], the one of Mundim et al. [23] and the BOP potential [26] are quite high compared to the experimental results and too low for the potential derived by Juslin and co-workers [24]. The potential derived by Xie and co-workers [22] seems also to overestimate this property by a large amount, however this may be due to the fact that during the evaluation of the vacancy formation energy, only the 1st nearest neighbours of the vacancies were allowed to relax, thus, the value obtained may not account for full relaxation. More problematic could be the fact that all the interatomic potentials predict that the di-vacancy is stable in disagreement with our *ab initio* calculations [35] and other unpublished *ab initio* calculations [48], but in agreement with yet other *ab initio* calculations [25]. It can be argued that if true, this fact simply shifts to slightly lower values (the first one being negative) the curve of the binding energy of a vacancy to vacancy clusters as a function of cluster size, so that it is not a key issue except when one wants to study thermal ageing, a process during which single vacancies travel in the matrix and can form di-vacancies and small vacancy clusters. This particular point will be further discussed in the section devoted to the parameterisation scheme and the *ab initio* results.

Regarding the vacancy migration energy, the experimental data lie between 1.7 eV [49] and 2.02 [50]. Note that according to Satta and collaborators [51], the extrapolation to 0 K of the experimental data leads to a migration energy of 1.50 eV. If one considers this large range of values, most potentials except the one derived by Xu [20] provide a good enough estimate of this property. Table 1 summarises the properties of the interatomic potentials investigated above.

2.2.3. He properties

There exist a few interatomic potentials able to model the interactions between tungsten and helium atoms. Wilson and Johnson [55] obtained a W–He potential by an approximate quantum mechanical method originally due to Wedepohl to study the properties of He interstitial and substitutional.

Caspers and co-workers [56] have determined activation energies for the interaction of He with vacancies and vacancy clusters using the W–He potential derived by Wilson and Johnson [55] by an approximate quantum mechanical method, and a He–He potential provided by Abrahamson [57]. Wilson and Bisson [58] have calculated specific helium tungsten defect configurations suggested by Kornelsen [59] to result from ion implantation following irradiation. They also used the W–He and W–W potentials derived by Johnson and Wilson [6] but the He–He was developed by Beck

Table 1
Relaxed vacancy formation E_v^{for} (eV) and migration energy E_v^{mig} (eV), as well as SIA formation energies $E^{for}_{\langle XXX\rangle}$ (eV) and migration energies E^{mig}_{SIA} (eV) obtained with empirical interatomic potentials. (s) stands for static calculations, (d) for dynamic calculations, the bold values indicate the most stable state predicted by each potential.

	E_v^{for} (eV)	E_v^{mig} (eV)	$E^{for}_{\langle 110\rangle}$ (eV)	$E^{for}_{\langle 111\rangle}$ (eV)	$E^{for}_{\langle 100\rangle}$ (eV)	$E^{for}_{crowdion}$ (eV)	E^{mig}_{SIA} (eV)
	Exp.	Exp.	*Ab initio*	*Ab initio*	*Ab initio*	*Ab initio*	Exp.
	3.1–4.0 [44]	1.7 [49]	9.84 [34]	**9.55** [34]	11.49 [34]	**9.55** [34]	See text
	4.0 [45]	2.02 [50]	10.2 [35]	**9.94 [35]**	11.88 [35]		
		1.50 at 0 K according to [51]					
[6]		1.44	**Most stable** [32]				0.38 (s)
							0.37 (d) [32]
[8]	3.60	2.0					
[9]	3.62 [10]	1.49 [10]	8.50 [10]	7.89 [10]	8.72 [10]	**7.86** [10]	
[12]			9.64 [12]	8.92 [12]	9.82 [12]	**8.89** [12]	0.027 (s) [12]
			9.71 [13]	9.02 [13]	9.88 [13]	**8.99** [13]	0.023 ± 0.006 (d) [52]
[14]	3.57 [53]	1.97 [53]		**1.8** [100] [54]			0.54 (d) [33]
[16]	4.1, 4.3						
[20]	3.57	2.34					
[22]	4.9						
[18]	3.95						
[23]	4.23	1.67					
[15]	3.74	1.55	**10.55**	11.87	13.79	12.00	
[24]	1.68		8.31				
[25]	3.56		9.841	9.550	11.513	9.557	0.013 [25]

[60]. Much more recently, Henriksson and co-workers [61] derived a new potential to simulate the initial stages of blistering in Helium implanted tungsten. The W–W interactions were obtained from the potential derived by Ackland and Thetford [12], the He–W interaction was obtained from an *ab initio* potential for the diatomic He–W diatom and the He–He potential was calculated using the DMOL package [62]. These potentials are surprisingly good as regards their predictions of the binding of He atoms with vacancies compared to the thermal desorption experiments available [63,56].

However, they all have the same flaw regarding the behaviour of He in interstitial configuration. Indeed, our *ab initio* calculations [64] predict that the most stable configuration for He in interstitial position is the tetrahedral site, as is also the case for Fe [65]. Contrary to the case of hydrogen or, more precisely deuterium (D), for which all experiments indicate that it occupies the tetrahedral site [66–68], no experimental data are available for the lattice location of He in tungsten, despite careful studies such as the ones of Picraux and co-workers [69]. This, according to Picraux and Vook [69] is due to the strong tendency for multiple helium trapping at defect centres presumed to be vacancies. The empirical potentials, as was the case for Fe [65], predict the octahedral site to be the most stable. In the case of Fe, Seletskaia and co-workers [70] explain the preferred interstitial location by an unexpected influence of magnetism on the properties of He in Fe. The introduction of He in a tetrahedral site induces less magnetic moment quenching than when the He atom is in an octahedral position. As the empirical potentials are not well suited to reproduce correctly the influence of magnetic properties (the electrons are not explicitly taken into account in such models) it is thus not so surprising that most of them fail to reproduce correctly the favoured position of He interstitials in Fe. The task is not impossible though, as a new three body potential as well as pair potentials [71,72] have been recently developed for Fe–He which predict correctly the stability of the He atom [73]. Similar to what was said about the SIA stability, the prediction of the correct interstitial site is not really important *per se*, however the consequences can be observed on the migration properties (of He). Indeed, the interatomic potentials predict the migration energy of He to be of the order of a few tenths of an eV, which corresponds to the difference in energy between the He in octahedral configuration and in a tetrahedral configuration. It could be argued that the predictions of the empirical potentials are in agreement with the experimental values of the diffusion coefficients of He [74,39]. However, we believe (and demonstrated in [64]) that this value does not correspond to the He migration energy as our *ab initio* calculations indicate that the lowest energy path to go from one tetrahedral site to another is not through the octahedral site and predict a migration energy of 0.06 eV, i.e. significantly lower than predicted by potentials. The results of our calculations indicate also, as, will be shown in the section devoted to the *ab initio* calculations, that another possible reason for the difficulty of establishing the most favoured interstitial site for He is the rapid formation of He–He clusters. As a conclusion to this brief overview, no potential at the moment appears to be capable of modelling correctly the behaviour of He atoms in a tungsten matrix. For this reason, the parameterisation of the OKMC model will be based on *ab initio* calculations as well as on a set of He desorption experiments. Furthermore, in the absence of a good W–He interatomic potential, the distribution of the He atoms and the primary damage created after implantation will be modelled using the Binary Collision Approximation (BCA) as described in the accompanying paper [1]. The BCA is designed to model the ballistic phase of cascades only. It is thus inappropriate to model the cooling phase of cascades as full MD does; however, a simple point defect recombination model, parameterised on full MD cascade simulations with semi-empirical potentials, may reasonably account for this. Alternatively, as is shown in [1], this recombination model may be tuned directly on experimental results.

2.3. Methodology followed to parameterise the OKMC code

2.3.1. Ab initio calculations used in the parameterisation

A large number of *ab initio* calculations in the framework of the Density Functional Theory were performed using the Vienna *Ab initio* Simulation Package VASP [75]. The calculations were done employing Blöchl's projector augmented-wave (PAW) method [76] within the Generalised Gradient Approximation (GGA) of Perdew and Wang [77]. The pseudo-potentials were taken from the VASP library. The supercell approach with periodic boundary conditions (PBC) was used to simulate point defects as well as pure phases. Brillouin zone sampling was performed using the Monkhorst and Pack scheme [78]. The plane wave cut-off energy was 350 eV in order to get converged results. 54 atom supercells with 125 kpoints as well as 128 atoms with 27 kpoints were used to check the convergence of the calculations with supercell size. For some specific cases, calculations with 250 atom supercells and 8 kpoints were also performed. For clarity and because the results were converged, only the results obtained with the largest atom supercell calculations will be presented in this article. All the structures have been relaxed by conjugate gradient, keeping the volume constant. The uncertainty on the *ab initio* results is 0.01 eV. Note, however, that different approximations or the use of pseudopotentials are likely to produce results that differ by more than 0.01 eV from these.

The binding energy E^{b}_{A-B} between A and B (where A is a cluster containing nHe atoms and B is a single He atom in the definition given above), is obtained as

$$E^{b}_{A-B} = [E(A) + E(B)] - [E(A+B) + E_{Ref.}] \quad (3)$$

where E(A) (resp. E(B)) is the energy of the supercell containing A only (resp. B), E(A + B) is the energy of the supercell containing both A and B in interaction with each other. This is done because of the limited size of the supercell which can be used (the cells are too small to be able to determine in one calculation the energy of a supercell containing the two entities not interacting with each other).

All the supercells contain the same number of metal sites, i.e. have the same size. Except when otherwise stated, the reference state $E_{Ref.}$ of the binding energies presented in this work is always the energy of a supercell without any defects, i.e. a perfect crystal.

2.3.2. He desorption experiments used in the parameterisation

Despite the fact that *ab initio* calculations are nowadays the most precise technique to determine the total energy of a set of atoms, as all numerical methods, they have limitations and uncertainties which must be kept in mind. One limitation of the *ab initio* calculations is the size of the supercells which can be used in a reasonable amount of time. The introduction of one vacancy in a 128 atom supercells can be perceived as being reasonable (even when periodic boundary conditions are used), but the study of clusters containing more than ten entities is more problematic even in 250 atom supercells. For these reasons, the parameterisation of the OKMC model relied also heavily on the experimental work of Soltan and co-workers [79], who, in a series of experiments, implanted He atoms in various amount and with various energies (0.25 keV, 0.4 keV, 1.69 keV and 3 keV) at 5 K in tungsten. These authors isochronally annealed the implanted specimen by increasing the temperature in logarithmic steps of $\frac{\Delta T}{T} = 0.2$ and $\frac{\Delta T}{T} = 0.5$ K with holding time of 240 s and 600 s, respectively. They monitored the change in the defect population as the temperature increased

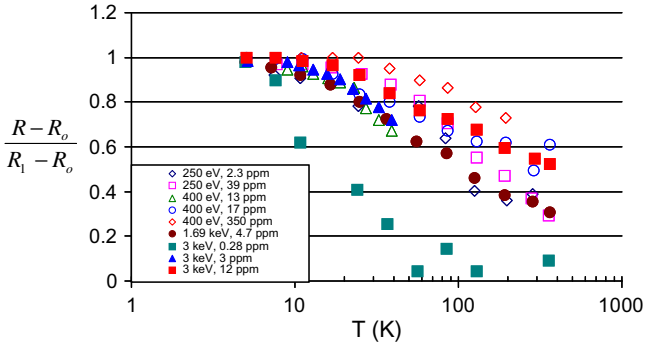

Fig. 2. Experimental resistivity recovery as a function of temperature for the nine experiments performed by Soltan and co-workers [79].

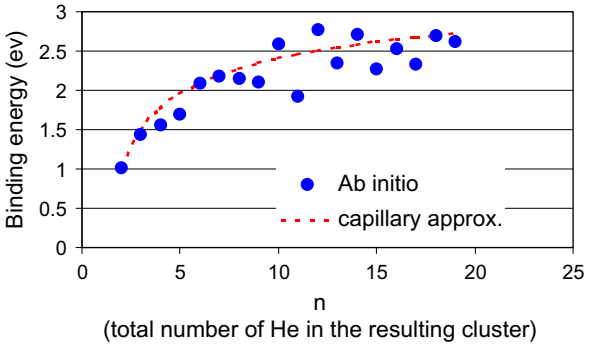

Fig. 3. Binding energy (eV) of one He atom to a cluster containing only He atoms, according to the following reaction $(n-1)\mathrm{He}+\mathrm{He}\rightarrow n\mathrm{He}$. All the He atoms are in interstitial configurations. The *ab initio* calculations were done using 250 atom supercells and eight kpoints.

by measuring the change in resistivity of the sample. The evolution of the resistivity versus temperature for the different He implantations performed are represented in Fig. 2.

2.3.3. Parameterisation of the pure helium objects

As already mentioned above, the *ab initio* calculations indicate that the most stable interstitial configuration for He is the tetrahedral site [64], the energy difference between the two possible interstitial sites ΔE_{T-O}, where O stands for octahedral, being equal to 0.22 eV. Furthermore, the substitutional configuration is 1.46 eV lower than the tetrahedral one.

The VASP code was used to determine the binding energies of one He atom to He clusters of size up to 18 He atoms and the results obtained are represented in Fig. 3. The binding energy between two He atoms is very high, close to 1 eV [64], and the results in Fig. 3 indicate also that the formation of He clusters without pre-existing damage is possible as was observed by Nicholson and Walls [80]. The most stable configuration for He atoms all in interstitial position is in a form of a platelet at least for clusters containing less than 10 He atoms at 0 K. The formation of He platelets was indeed observed in Mo by Evans [3] and in tungsten by Iwakiri et al. [81]. For larger size clusters, platelets are also stable, however more work is necessary to determine the most stable configurations and in particular to find out when trap mutation (the emission of a SIA leaving a vacant site, i.e. more open space for the He atoms to occupy), should take place. Preliminary calculations indicate that trap mutation does not take place as easily as in Fe, i.e. for five He atoms very probably because W is a stiffer materials than Fe, and the formation energy of a SIA is higher.

The data of Fig. 3 were used in the OKMC model. At larger cluster sizes (i.e. for clusters containing more than 18 He atoms), a capillary approximation was used.[1]

As regards the mobilities, the *ab initio* calculations indicate that He migration energy as an interstitial is very low, around 0.06 eV. We showed in [64] that the disagreement with the experimental values can be explained by the fact that an isolated He atom diffuses very quickly in the tungsten matrix and as soon as it will encounter another He atom, it will be strongly bind to it, so that the experimental migration energies determined in [74,39] are very probably migration energies of small He clusters rather than of isolated He atoms. This is in perfect agreement with the results of Soltan and co-workers [79] who demonstrated that concentrations as low as 350 ppm of He suppressed He migration as can be seen on Fig. 2, because, they state, of the clustering of these elements. They furthermore calculated that in the experiments of Wagner and Seidman [74] as well as that of Amano and Seidman [39], the concentration of implanted He was 5%. They thus explain why, in their own experiments, He becomes mobile at temperature below 5 K, in contradiction to the previous results [74] and [39] where mobility of ^{3}He and ^{4}He was observed only above 90 K.

A close examination of the experimental results of Fig. 2 indicates that the He atoms seem to be already moving at 5 K, as can be deduced from the decrease in the resistivity data for the 400 eV He implanted in low concentrations (13 and 17 ppm). According to our model, this implies that their migration energy is even lower than the value of 0.06 eV that was found in our *ab initio* calculations [64]. To reproduce the low concentration results, we thus set the mobility of the He atom to 0.01 eV and decreased the mobility of the He clusters depending on their sizes according to the law represented in Fig. 4. We did check using *ab initio* molecular dynamics calculations that small He clusters were indeed mobile.

Using the He parameters presented above, we simulated the two He desorption experiments below threshold featured in Fig. 2. The OKMC simulations, as the experiments, consist in two parts, the implantation sequence followed by the isochronal annealing. 13 appm and 350 appm of 400 eV He were implanted at 5 K in thin films of W of dimension $399\times400\times1001$ in lattice units. Periodic boundary conditions (PBC) were applied in two of the three directions, simulating a thin foil of tungsten, 317.3 nm thick. The surface orientation of the single crystal simulated is always perpendicular to the $\langle0\,0\,1\rangle$ direction. The experimental implantation rate was $10^{15}\,\mathrm{s}^{-1}\,\mathrm{m}^{-2}$ [82] which corresponds to the introduction of 16 He per second in the simulation box. For

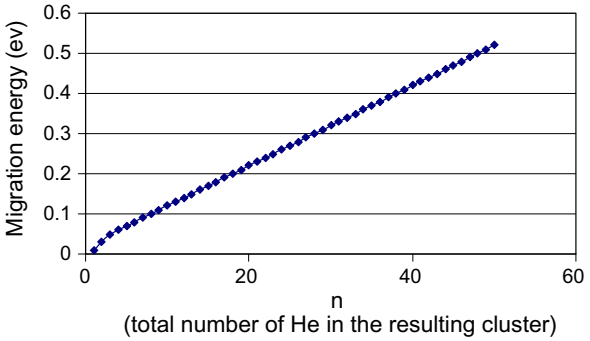

Fig. 4. Mobility law for small He clusters.

[1] The capillary law is an empirical model assuming that the defect cluster containing n atoms is a spherical object, whose formation energy is proportional to the surface of the cluster. With this approximation, the binding energy $E^b(n)$ corresponding to adding an atom to a cluster of size $n-1$ is given by $E^b(n\rightarrow(n-1)+1)=E^{for}(n-1)+E^{for}(1)-E^{for}(n)=\left[\left(E^b(2)-E^{for}(1)\right)((n)^{2/3}-(n-1)^{2/3})\right]/\left(2^{2/3}-1\right)+E^{for}(1)$. When n becomes large the asymptotic limit will be $E^{for}(n=1)$.

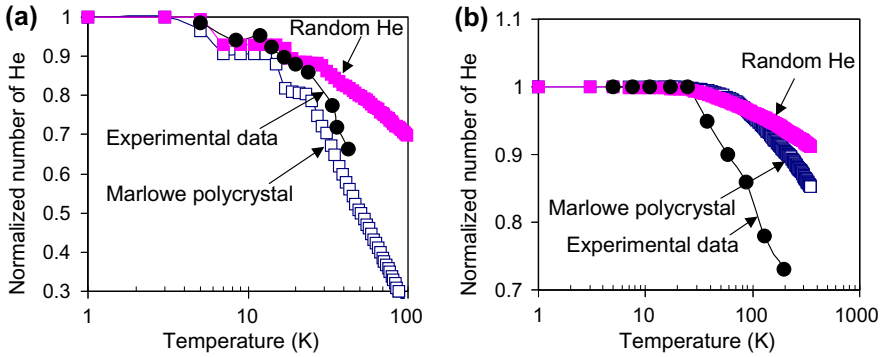

Fig. 5. OKMC simulations of under-threshold He desorption experiments: 13 ppm (a) and 350 ppm (b) of 400 eV He atoms were introduced either completely at random in the 399 × 401 × 1001 (in lattice units) simulation box or according to the distribution profile determined using Marlowe (see accompanying paper for more details). The experimental results are the ones presented in Fig. 2.

each of the two experiments, two sets of implantations were done. One was obtained by introducing a spatially random flux of He atoms (curves labelled "random He" in Fig. 5) while for the second set, He was distributed according to the Marlowe results, considering that the tungsten matrix is crystalline (curves labelled "Marlowe polycrystal" in Fig. 5). See the companion paper [1] for more explanations. An isochronal annealing of the whole box was then simulated by increasing the temperature by steps of 2 K every 60 s (we checked that, for these simulations, a logarithmic increase of the temperature leads to similar results as a linear temperature program). The use of longer time steps does not change the results either. As the simulations are very short and the volume simulated very small as compared to the experimental sample, five simulations were done for each case, changing the seed of the random number generator. Fig. 6 represents the evolution of the relative total number of defects (a cluster of size 4 corresponding to four defects in the plot) versus temperature as compared to the experimental results. The reference is the total number of defects at the beginning of the isochronal sequence. Indeed, as the implantation was performed at 5 K, a temperature at which the isolated He atoms are already mobile, a few He atoms reached the surface and left the box before the start of the isochronal sequence (respectively, 13.2% and 10.7% for 13 ppm and 350 ppm).

The agreement between the experimental results and the OKMC data is rather good, specially as they reproduce the shift in He desorption observed for the higher dose implantation due to the formation of He clusters. At larger doses however, the desorption rate is underestimated. A different mobility law has been tested for the migration energy of He clusters versus size. The law was not linear, but had instead an exponent <1 and the migration energy saturated around 0.35 eV. This new law lead to a stiffer slope but it did not modify the offset. A close examination of the results indicate that 6% of the implanted He are in the form of clusters of size smaller or equal to three and in order for desorption to occur faster, and to be thus more in agreement with the experimental results, these clusters should reach the surface more easily. *Ab initio* calculations of small clusters motion is currently under investigation.

In the temperature range explored in these simulations, the only events that take place are migration events (and formation of clusters through local reactions). No emission from clusters happens as the binding energies are too high. Because of the monotonic increase of the cluster migration energy, each cluster size family starts moving at a different temperature. For the 13 ppm experiment, most of the moving objects reach the surface before they have a chance to meet another object. On the desorption curves, mainly two steps are observed: one around 5 K and the second one at 15 K. The first step corresponds to the desorption of the mono-He atoms and the second is due to the 2He clusters desorption. These steps are smaller in the 350 ppm experiment than in 13 ppm first because more clustering takes place, secondly because, as is visible on the size distribution of the implanted damage, mono-He and 2He represent only 2% of the initial amount of He. Those steps are then followed by a monotonous decrease due to the motion and desorption of bigger size clusters. It is important to emphasise that this agreement can only be reached if the He atoms are properly introduced in the box before the annealing

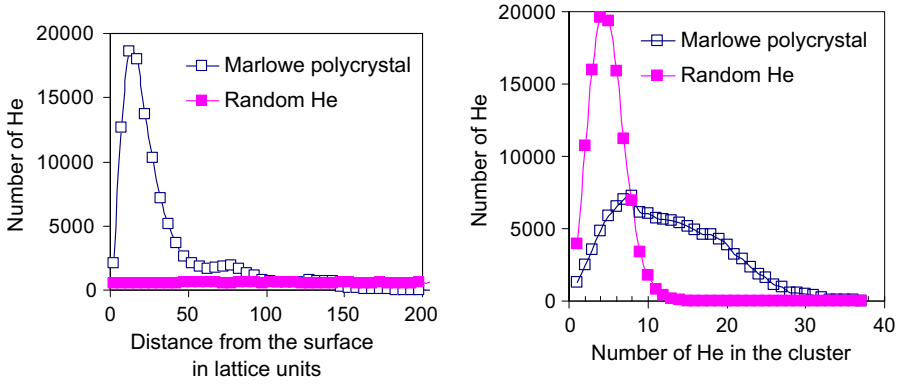

Fig. 6. Mean spatial distribution of the He atoms along the *z* coordinate of the box, for the 350 ppm experiment at the end of implantation. The He atoms were introduced either completely at random in the 399 × 401 × 1001 (in lattice units) simulation box or according to the distribution profile determined using Marlowe. Right hand side figure, the abscissa is the number of He atoms found in clusters of given size.

simulations. This can be understood by looking at the initial He spatial profile in the box for the two cases which is provided in Fig. 6 for the 350 ppm experiment. The delay observed between the desorption of the He after the random and thus homogeneous implantation is due to the larger mean distance between the He objects and the surface. Indeed, the more jumps the He objects have to perform to reach the surface, the larger their probability to meet another cluster. Isochronal annealing sequences using 10,000 times longer time steps were simulated to check that this was not a "step time effect" and only a slight increase of the amount of desorption was observed.

The cluster size distribution evolves during the isochronal annealing. Indeed, when the clusters of one specific size family start to move, some of them reach the surface and leave the simulation box, while others, meeting other clusters, stop moving to become part of a bigger cluster. In Figs. 7 and 8 the cluster size populations are provided at temperatures corresponding respectively to the initial conditions, after the mono-He desorption (11 K), after the desorption of the 2He clusters (21 K) and later in the simulation (41 K, 101 K and 201 K).

For the 13 ppm experiment, the initial distribution (Fig. 7) is larger for the implantation done using the Marlowe implantation profiles because the He atoms are introduced closer to each other than in the random distribution, and as they can already move a little at 5 K, some clusters are found to form almost immediately. At 11 K, the cluster size distributions are similar but above 21 K bigger size clusters are formed with the "random He distribution" than with the "Marlowe polycrystal".

For the 350 ppm experiment, the initial cluster size distribution is much wider for the implantation done with the Marlowe implantation profiles. As a consequence there are less very small size clusters (i.e. the clusters which start moving at the very beginning of the annealing sequence), than in the "Random He" as can be seen in Fig. 8. This explains why the first steps in the desorption curve are more pronounced in the latter case. Step by step the smallest size clusters leave the simulation box and a slight increase of the bigger size cluster families is observed. With the random He implantation, the initial distribution is tighter, the distribution broadens and reaches the width of the Marlowe cascade implantation distribution only above 101 K.

The decreasing slope is in good agreement with the experimental data for the "Marlowe polycrystal" implantation, however it starts at 55 K rather than 25 K. This is probably due to the balance between clustering and desorption and this point has to be further explored. Nevertheless, the results of the simulations of under-threshold He desorption leads us to conclude that the parameterisation of the pure He objects is rather satisfactory.

2.3.4. Parameterisation of the pure vacancy objects

The vacancy formation energy obtained with the VASP code is 3.23 eV for a 250 atom supercell simulation. It lies within the experimental range 3.1 eV [44] and 4.0 eV [44,45].

As regards the formation of vacancy clusters, very interestingly, our calculations predict that the di-vacancy is not stable: two vacancies repulse each other even when they are situated as far as in 5th nearest neighbour position [35], while for vacancy

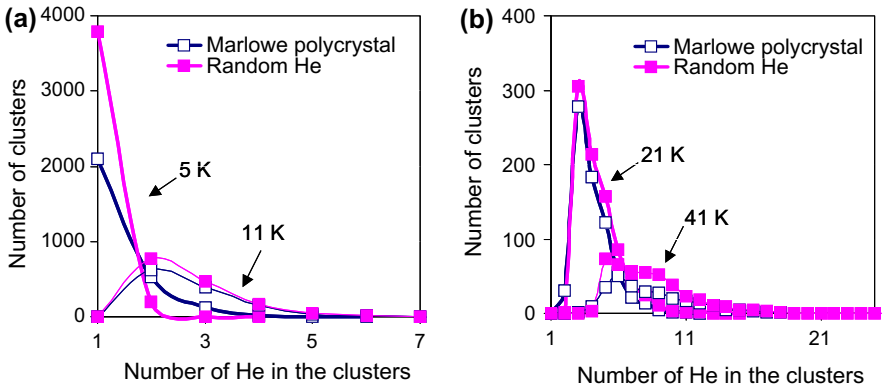

Fig. 7. Cluster size distributions for different temperatures (5 K and 11 K (a) and 21 K and 41 K (b)) during the OKMC simulations of under-threshold He desorption experiments. He atoms (13 ppm of 400 eV) were introduced either according to the distribution profile determined using Marlowe or completely at random.

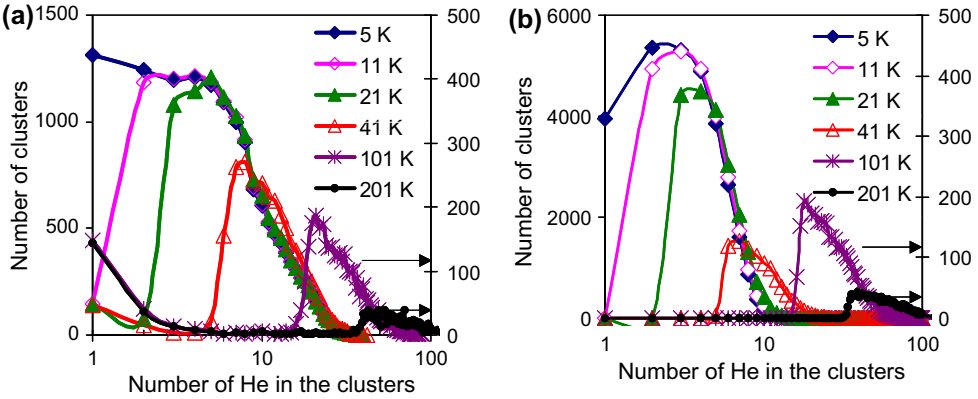

Fig. 8. Cluster size distribution in OKMC simulations of under-threshold He desorption experiments. He atoms (350 ppm of 400 eV) were introduced either according to the distribution profile determined using Marlowe polycrystal: (a) either completely at random (b). The curves corresponding to the highest two temperatures have been blown up and should be read on the secondary axis.

Table 2
Binding energies (eV) of one vacancy to a vacancy cluster of size $(m-1)$ according to the following reaction $(m-1)v + v \rightarrow mv$. The *ab initio* calculations were done using 250 atom supercells and eight kpoints.

m	$E^b_{V-(m-1)V}$ (eV)
2	−0.1
3	0.04
4	0.64
5	0.72
6	0.89
7	0.72
8	0.88
>8	Capillary approximation

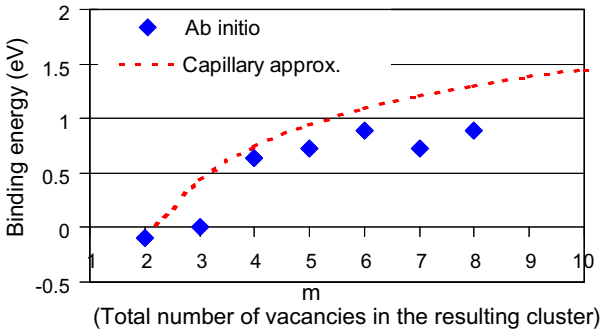

Fig. 9. Binding energy (eV) of one vacancy to a vacancy cluster according to the reaction $(m-1)v + v \rightarrow mv$.

clusters, the binding energy of a vacancy to a vacancy cluster becomes positive only when the final cluster size is larger than 3 as can be seen in Table 2 and Fig. 9. This is in contradiction with the data predicted by other groups. However, most of these results were obtained by either empirical potentials [8,63,15] or semi-empirical calculations as in [83]. Mundim and collaborators' potential obtained with a recursive procedure from *ab initio* calculations are the only ones to predict a negative binding energy for the di-vacancy situated in first nearest neighbour position in partial agreement with our results. One must add also that more recent *ab initio* calculations using the software PLATO are in contradiction with our finding as the authors of [25] obtained a positive binding energy of 0.41 eV for the di-vacancy binding energy. It is a little difficult at first to conciliate our finding that di-vacancies are not stable with the vacancy loops observed by Transmission Electron Microscopy [84–88] or the voids observed in displacement cascades by FIM [89]. However, in the case of displacement cascades, lots of vacancies are created in the core of the damaged region, which are already very close to each other, and thus the formation of vacancy clusters can take place by immediate agglomeration of vacancies without going through the process of first creating a di-vacancy, which will be joined by a vacancy to form a tri-vacancy and so on.

Another plausible scenario is the stabilisation of the di-vacancy by impurities. The most likely candidate is C which is a typical impurity found in bcc metals and whose prominent influence on point-defect properties, specially the vacancies is demonstrated in the isochronal experiments of Takaki et al. [90] (in Fe), or in the positron annihilation experiment of Vehanen et al. [91] and is now commonly accepted. We determined the total binding energy of two vacancies and a C atom and the value obtained (3.23 eV for a 128 atom supercell) does confirm that C atoms can stabilise di-vacancies. In a very recent work, Kato found that H also stabilises the di-vacancy [92]. In that regard, one can then add that the empirical potentials which predict stable di-vacancies in an unrealistically pure W matrix can then be considered as taking into account in an indirect manner the influence of impurities.

Regarding the migration of vacancy objects, we obtained a vacancy migration energy (1.66 eV for a 128 atom supercell [35]) in very good agreement with the experimental data which lie between 1.7 eV [49] and 2.02 [50]. We used thus this value in our model. Let's add that all our *ab initio* calculations are done at 0 K, while the experimental data have been obtained at high temperatures, thus the data should be in theory compared with the value extrapolated at 0 K, 1.50 eV [51]. All vacancy clusters are in principle allowed to move but their diffusion coefficients are so low, that their motion during the isochronal annealing experiment is negligible.

2.3.5. Parameterisation of mixed vacancy Helium objects

The binding energy of a single He atom or a single vacancy with small He-vacancy complexes $He_n{\cdot}v_m$ as obtained *ab initio* for clusters of up to size 4 can be found in [93]. This database has been increased and the results for larger clusters are shown in Fig. 10.

The data in Fig. 10 indicates that when n and m are close to one another, a He atom binds more strongly with a mixed He-vacancy cluster than a vacancy to a cluster of same composition. When the number of He atoms in the cluster is larger than that of vacancies, the removing of one vacancy becomes very costly. For larger size clusters, no emission can take place.

The binding energy between a single vacancy and He is very high, and thus the dissociation of such a cluster is highly improbable. However when a SIA moves close to this complex, the W atom jumps in the vacancy and the He atom moves to a tetrahedral site and will then be able to migrate very quickly. This reaction was checked using *ab initio* molecular dynamics and is taken into account in our model. The possibility of He motion through the help of two vacancies, which was found to be energetically costly in Fe [65], was not investigated as the He·2v complex does not appear to be very stable. The He and vacancy clustering data are usually represented in terms of dissociation energy (i.e. the sum of the migration energy and the binding energy) of a vacancy or an interstitial He versus the ratio of He to vacancy. This is presented in Fig. 11. The dissociation energy at the cross-over between the two curves is close to 4 eV and the He to vacancy ratio is one. The mobility of all the mixed nHe·mv objects was set to zero.

2.3.6. Parameterisation of self-interstitial atoms and self-interstitial atom clusters

As pointed out earlier in this paper, the SIA migration energy is quite a debated question and we used what we believe to be the most up-to-date results which are those obtained with one of the most recent empirical potential derived from *ab initio* calculations [25]. The SIA moves thus along ⟨1 1 1⟩ directions with a migration energy of 0.013 eV, and changes direction with a rotation energy of 0.38 eV, as was determined in [25]. The SIA clusters also move with the migration energy of 0.013 eV along a ⟨1 1 1⟩ direction [42], but they cannot change directions. The linear dependence of the diffusion coefficient with temperature demonstrated in [25] has not been included in the model. The binding energy of a SIA with a cluster of SIAs has been determined using VASP for a cluster size up to 7 SIAs (Fig. 12 and Table 3). The binding energies are high, indicating that SIA clusters will emit SIA only at elevated temperatures.

2.3.7. Parameterisation of mixed SIA helium objects

Our *ab initio* calculations indicate that a He atom close to a ⟨1 1 1⟩ dumbbell binds the most strongly to it when the ⟨1 1 1⟩ dumbbell rotates to become a ⟨2 2 1⟩ dumbbell. In this configuration, the He atom moves slightly away from the tetrahedral site

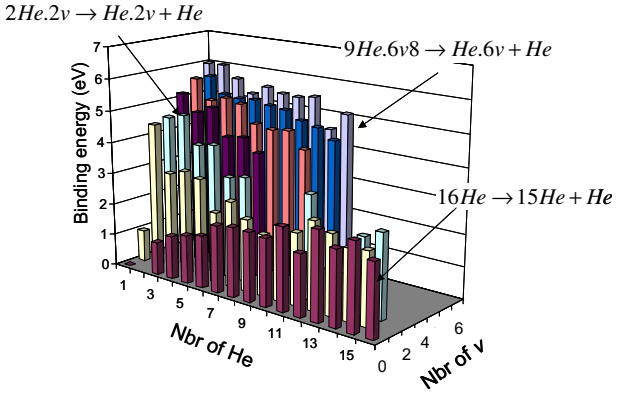

(a) *Binding energies (eV) for the reaction:* $nHe.mv \rightarrow (n-1)He.mv + He$.

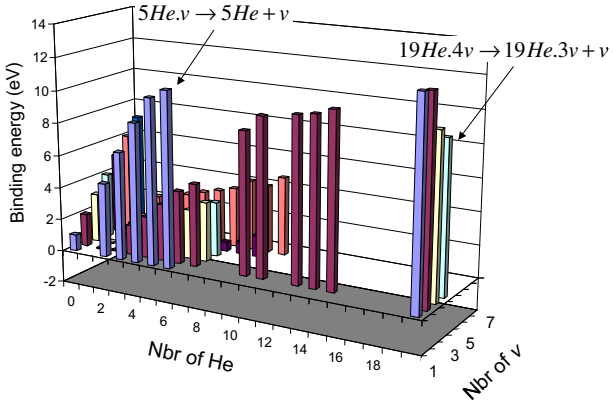

(b) *Binding energies (eV) for the reaction:* $nHe.mv \rightarrow nHe.(m-1)v + v$.

Fig. 10. Binding energies (eV) for the formation of mixed *n*He·*m*v clusters.

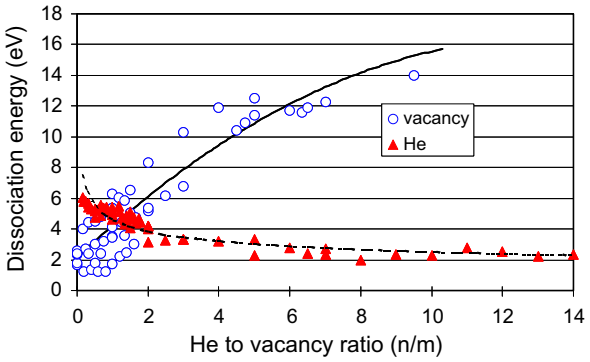

Fig. 11. Dissociation energies of a He atom or a vacancy from *n*He·*m*v clusters as a function of He to vacancy ratio.

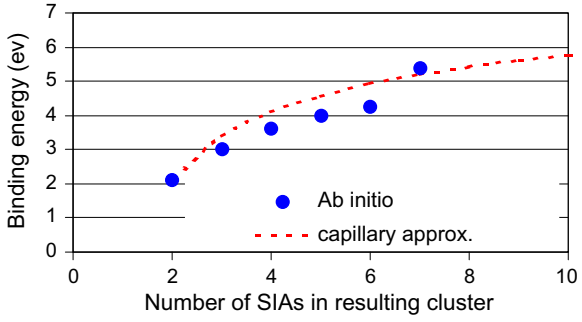

Fig. 12. Binding energy (eV) of one SIA to a SIA cluster.

and the resulting binding energy is 0.94 eV, which is very close to the binding energy between two He atoms (1 eV). Some configurations for which the dumbbell remains ⟨1 1 1⟩ or the He atom remains close to their octahedral initial positions are stable or metastable but the binding energy is not as high. In the model, mixed He SIA (up to size 10) are thus bound with a binding energy of 0.94 eV, this energy does not depend on the cluster size, and they cannot move.

2.3.8. Influence of impurities

Impurities even in small amount play a crucial role as they can bind with the point defects and change their mobility. In the code, impurities are introduced as traps for the moving species. These

Table 3
Binding energies (eV) of one SIA to a SIA cluster of size m according to the following reaction $(m-1)\mathrm{I} + \mathrm{I} \rightarrow m\mathrm{I}$. The *ab initio* calculations were done using 250 atom supercells and eight kpoints. The clusters are formed of parallel ⟨1 1 1⟩ SIAs.

m	$E^{b}_{\mathrm{I}-(m-1)\mathrm{I}}$ (eV)
2	2.12
3	3.02
4	3.60
5	3.98
6	4.27
7	5.39
>7	Capillary approximation

Table 4
Binding energies (eV) of the "impurities" with the moving objects: the *ab initio* calculations were done using 128 atoms supercells and 27 kpoints.

Moving species	Impurity type				
	H	He	C	Mo	Re
SIA	0.33	0.94	0.62	0.44	0.80
v	1.22	4.57	2.01	0.04	0.23
He	0.20	1.03	0.37	0.21	0.02
2He	0.32	1.36	0.54	0.34	0.26
3He	0.41	1.52	0.73	0.48	0.51

traps are characterised by their capture radii and binding energies. The binding energies were determined using *ab initio* calculations for a few possible impurities and are presented in Table 4. Among all the possible impurities, it was decided to investigate the possible influence of: (i) C as its prominent role in bcc metals is well known, (ii) Mo as it is the native impurity of W, (iii) Re as it can be obtained by transmutation of W. Furthermore it is commonly used as an alloying element of W to increase its re-crystallisation temperature and its ductility. H which will impinge on the surface of the divertor as well as He was also investigated.

C binds very strongly with both the vacancy and the SIA which is not the case in Fe, where C binds with SIAs only when they are quite far apart [94]. H binds with both vacancies and SIAs. The binding energy with H is not negligible: 0.20 eV, and in a previous work, it was shown that H binds also very strongly with He clusters [93], in agreement with the experimental findings that He pre-irradiation of metals efficiently enhances the retention of hydrogen isotopes in the penetrated region [95,96].

Mo does not appear to establish any interactions with vacancies, contrarily to Re whose binding energy with the vacancy is around 0.2 eV. Mo and Re establish strong interactions with the SIAs as can be seen from Table 4 and their most stable configuration in the vicinity of a dumbbell is as a mixed dumbbell. Mixed dumbbells in metals can be very mobile and transport solute atoms throughout the tungsten matrix. Our results indicate that Re establishes attractive interactions with both vacancies and self-interstitials. These results are in very good agreement with the general finding that, under irradiation, radiation induced precipitation of WRe alloys are observed [97–100,22], even if this needs to be corroborated by the determination of the corresponding migration energies. Note that the SIAs in tungsten being crowdions rather than dumbbells, it is more difficult to imagine how they can play a role in the transport of chemical species, but their behaviour will be nevertheless modified by these solute elements.

In this work, traps were introduced which act only on the moving defects containing either a vacancy or an interstitial.

Tables 5–7 summarise the different formula used to determine the capture radii as well as migration energies and binding energies. The formula and rationale behind the formula are very similar to the ones detailed in [2] for the SIAs and the vacancies. For the He objects, the nearest neighbour distance between He atoms in a cluster was determined from the position of the He atoms in a platelet. Note that although some objects can be anisotropic, as for instance the He platelets, they are, in this work, treated as being isotropic, i.e. their capture volumes are spheres. The He–He distance in the platelet as obtained by *ab initio* calculations, allows us to approximate the volume of a nHe platelet by a sphere of "density" of nHe atoms per bcc unit cell.

Table 5
Capture radii associated to different objects as a function of object size (expressed by the integer numbers n, m, p and q). $r_0 = \sqrt{3}a_0/4$, i.e. half the 1st nearest neighbour distance (with $a_0 = 3.17$ Å). $r_1 = 3$ Å. $\sqrt{3}a_2/4 = 0.8$ Å. The bias factor for SIAs is $\gamma = 1.15$. Note that ε denotes an arbitrary, small, positive correction to the exact values $r_{\mathrm{trap}} = 5$ Å.

Object	Capture radius
mI $m \geqslant 1$	$r_{m\mathrm{I}} = \gamma[(r_0+\varepsilon) + (\frac{3}{4\pi}\frac{a_0^3}{2}m)^{1/3} - (\frac{3}{4\pi}\frac{a_0^3}{2})^{1/3}]$
mv $m \geqslant 1$	$r_{m\mathrm{v}} = (r_0+\varepsilon) + (\frac{3}{4\pi}\frac{a_0^3}{2}m)^{1/3} - (\frac{3}{4\pi}\frac{a_0^3}{2})^{1/3}$
nHe $n \geqslant 1$	$r_{n\mathrm{He}} = (r_1+\varepsilon) + (\frac{3}{4\pi}\frac{a_0^3}{10}n)^{1/3} - (\frac{3}{4\pi}\frac{a_0^3}{10})^{1/3}$
nHe·mv $m \geqslant 1$, $n \geqslant 1$	$r_{n\mathrm{He}\cdot m\mathrm{v}} = r_{m\mathrm{v}}$
nHe·mI $m \geqslant 1$, $n \geqslant 1$	$r_{n\mathrm{He}\cdot m\mathrm{I}} = r_{m\mathrm{I}}$
Traps	$r_{trap} + \varepsilon$

Table 6
Parameters for object migration. All the clusters, but the mixed ones, are mobile. The values of the constants are $\nu_0 = 6 \times 10^{12}$ s^{-1}, $q = 1000$ and $s = 0.5$.

	Attempt frequency, ν (s^{-1})	Migration energy E^{mig} (eV)	Comment
Single vacancy	ν_0	1.66	3D motion
mv; $m > 1$	$\nu_0\,(q^{-1})^{n-1}$	1.66	3D motion
Single SIA	ν_0	0.013	1D motion along ⟨1 1 1⟩, $E_{\mathrm{rot}} = 0.38$ eV
mI; $m > 1$	$\nu_0 \cdot m^{-s}$	0.013	1D motion
Single FIA	$10^{-2}\,\nu_0$	0.01	3D motion
nHe; $n = 2$	$10^{-2}\,\nu_0$	0.03	3D motion
nHe; $n = 3$	$10^{-2}\,\nu_0$	0.05	3D motion
nHe; $n > 3$	$10^{-2}\,\nu_0$	$E^{\mathrm{mig}}_{(n-1)\mathrm{He}} + 0.01$	3D motion

Table 7
constants used in the capillary laws for the calculation of the binding energies of different elementary defects to clusters of different sizes.

Object	E^{b} (eV)	E^{for} (eV)
$E^{b}_{\mathrm{v}-(m-1)\mathrm{v}}$	−0.1	3.23
$E^{b}_{I-(m-1)\mathrm{I}}$	2.12	9.96
$E^{b}_{\mathrm{He}-(n-1)\mathrm{He}}$	1.02	4

2.4. OKMC simulations of above-threshold He desorption experiments

Using the parameters presented above, we simulated above-threshold He desorption experiments and more precisely the desorption of 12 ppm of 3 keV He atoms. Two implantations were

done. In one case, the implantation was done by introducing cascade debris obtained with the Marlowe code parameterised as described in the companion paper [1]. According to Marlowe, a 3 keV He atom creates on average 0.29 FP as can be seen Table 1 of [1]. In the second case, the same conditions were used but the location of the He implanted He atoms and of the FPs were selected at random. The experimental implantation rate was 10^{15} s^{-1} m^{-2} [82] which corresponds to the introduction of 16 He per second in the simulation box. For the two first sets of simulations, we thus introduced 16 "Marlowe cascades" or 16 He atoms for the random case per second and the corresponding amount of FP. For these simulations, 100 ppm C atoms were introduced as static traps acting on SIAs and vacancies as well as their clusters. The results are presented in Fig. 13, where once again a good agreement is obtained when the He distribution and the associated primary damage is correctly introduced, i.e. when the spatial correlation between the implanted He atoms and the point defects created are taken into account. When the He atoms and the associated damage are introduced in the simulation box according to the prediction of Marlowe taking into account the fact that W is a crystal (see companion paper [1] for more details on this particular aspect), the evolution of the total number of defects in the box follows quite nicely the experimental results of Soltan et al. [79]. The decrease in the number of defects appearing before 10 K and around 15 K corresponds, as in the case of the threshold simulations, to the desorption of mono-He atoms and 2He clusters. However, in that case, some of these clusters become trapped by SIAs or vacancies, and the number of He atoms leaving the box is thus reduced as compared to the under-threshold simulations. The He atoms meeting a SIA or a vacancy stop moving to form a mixed cluster. As a result, the decrease in the total number of defects for the low temperatures is less significant for the 3 keV He than for the 400 eV He implantations. Note also that, similarly to the case of the below energy threshold experiment, the total amount of defects introduced during the implantation is not available for the isochronal annealing sequence. Indeed at 5 K, both He atoms and SIAs can move and thus a certain amount of SIAs recombined with vacancies, some bound to He atoms, while a few of them left the box along with a few He atoms.

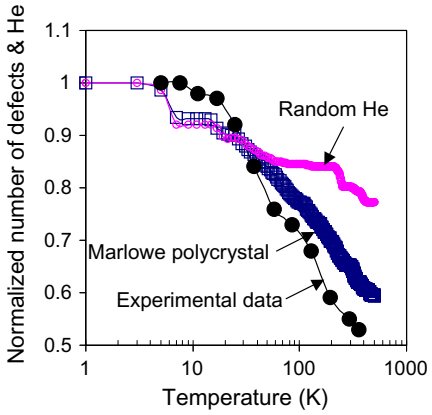

Fig. 13. OKMC simulation of above-threshold He desorption experiment. 12 ppm of 3 keV He and the vacancies and SIAs created during the process were introduced either completely at random in the 399 × 401 × 1001 (in lattice units) simulation box or according to the distribution profile determined using Marlowe (see accompanying paper for more details). C atoms (100 ppm) were introduced as traps for SIAs and vacancies as well as their clusters. The experimental results are the ones from Fig. 2.

Above 200 K, the SIAs captured in the C traps are released and more mono-vacancies are thus annihilated, however, some SIAs remain as mixed SIA-He clusters which do not move. At 500 K the microstructure consists of mono-vacancies and mono-SIAs (respectively around 90% and 30% of the initial number), 20% of the vacancies and 100% of the SIAs are in mixed clusters, all the He are in mixed clusters (trapped half by vacancies and half by interstitials) and 30% of them contain more than 10 He atoms. A typical cluster distribution is represented in Fig. 14 at 250 K. The significant result in these simulations is that it is important to model the implantation profile correctly. A close examination of the data indicates that the main difference between the "Marlowe polycrystal" and "random defects" is due to the fact that clustering, i.e. the formation of large pure He clusters is less efficient for the "Marlowe polycrystal", whereas more mixed clusters form for the "random defects" simulations. At 100 K all the He atoms are trapped on both mono-SIA and mono-vacancies in the "random defects" simulations while this is the case only above 500 K for the "Marlowe polycrystal simulations". The mixed objects are not mobile, and the He atoms are thus trapped, while the pure He defects are mobile and can leave the simulation box.

To summarise, the overall evolution of the number of defects in the box versus temperature is quite close to the experimental data provided that the implantation profile is correctly modelled. Our simulations indicate that He desorption results from a competition between the formation of mobile clusters and sessile ones. Let's add that, in our model, pure He clusters are mobile whatever their

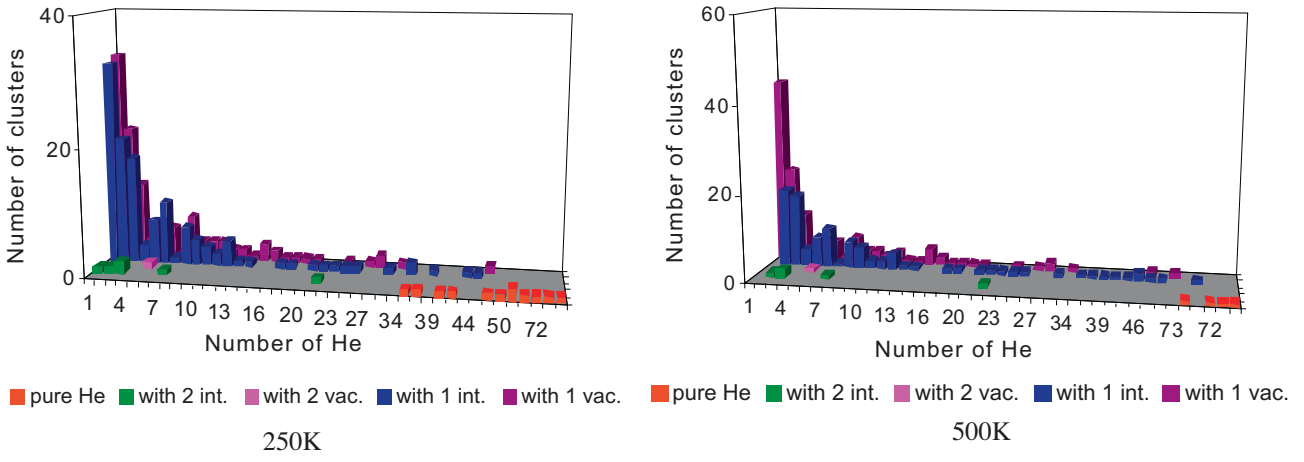

Fig. 14. Histogram of the number of He clusters in function of the number of He for mixed clusters with, respectively, 0, 1 and 2 vacancies or interstitials. These values have been obtained for one of the typical OKMC simulation of above-threshold He desorption experiment with "Marlowe polycrystal".

size. This is not very physical as trap mutation should occur. However, our calculations indicate that, contrarily to the case of Fe or Mo, the punch-loop mechanism whereby a vacancy or a void associated with a SIA or a SIA loop forms and thus traps the He cluster because of the pressure induced, will take place for He clusters containing more than 10 He atoms because tungsten is a very stiff materials. Therefore there will be quite many families of mobile He clusters in the tungsten matrix. On the other hand, as the *ab initio* calculations indicate that He clusters can be trapped by impurities, this needs to be included in the model as well.

3. Conclusions

The data set obtained thanks to *ab initio* calculations has been extended compared to previous work [93] and used to simulate isochronal annealing experiments of He desorption from W.

He atoms bind with self-interstitial atoms, vacancies, impurities, hydrogen and with other He atoms in this metal. The *ab initio* based parameterisation is able to reproduce correctly the evolution of the defect population during the He desorption experiment provided that the implantation profile is correctly modelled.

Furthermore, induced defects act as traps for the otherwise very mobile He at low temperature, inhibiting He desorption. Because He desorption results from a competition between mobile and sessile clusters, it is thus very important to model properly their distribution, i.e. the primary damage.

Acknowledgement

The authors wish to thank P. Jung for his comments. This work is supported by CEA under the collaborative contract number V 3542.001 on Fusion engineering issues, as well as CNRS under the programme interdisciplinaire énergie CHETEX. This research has been done using the CRI supercomputer of the Université Lille1 – Sciences et Technologies supported by the Fonds Européens de Développement Régional.

References

[1] M. Hou, C. Ortiz, C.S. Becquart, C. Domain, U. Sarkar, A. Debacker, Companion Paper.
[2] C. Domain, C.S. Becquart, L. Malerba, J. Nucl. Mater. 335 (2004) 121.
[3] J.H. Evans, A. Van Veen, L.M. Caspers, Nature 291 (1981) 310.
[4] W.M. Young, E.W. Elcock, Proc. Phys. Soc. 89 (1966) 735.
[5] A.B. Bortz, M.H. Kalos, L. Lebowitz, J. Comp. Phys. 17 (1975) 10.
[6] R.A. Johnson, W.D. Wilson, in: P.C. Gehlen, J.R. Beeler, R.I. Jaffee (Eds.), Interatomic Potentials and Simulation of Lattice Defects, Plenum, New York, 1972, p. 301.
[7] R.A. Johnson, P.J. White, Phys. Rev. B 18 (1978) 2940.
[8] R.A. Johnson, Phys. Rev. B 27 (1983) 2014.
[9] M.W. Finnis, J.E. Sinclair, Philos. Mag. A 50 (1984) 45.
[10] J.M. Harder, D.J. Bacon, Philos. Mag. A 54 (1986) 651.
[11] G.J. Ackland, M.W. Finnis, Philos. Mag. A 54 (1986) 301.
[12] G.J. Ackland, R. Thetford, Philos. Mag. A 56 (1987) 15.
[13] J.M. Harder, D.J. Bacon, Philos. Mag. A 58 (1988) 165.
[14] R.A. Johnson, D.J. Oh, J. Mater. Res. 4 (1989) 1195.
[15] W. Hu, W. Shu, B. Zhang, Comput. Mater. Sci. 23 (2002) 175.
[16] A.E. Carlsson, Mater. Res. Soc. Symp. Proc. 209 (1991) 165.
[17] M.I. Baskes, Phys. Rev. B 46 (1992) 2727.
[18] B.J. Lee, M.I. Baskes, H. Kim, Y.K. Choo, Phys. Rev. B 64 (2001) 184102.
[19] S.M. Foiles, Phys. Rev. B 48 (1993) 4287.
[20] W. Xu, J.B. Adams, Surf. Sci. 301 (1994) 371.
[21] Y.R. Wang, D.B. Boercker, J. Appl. Phys. 78 (1995) 123.
[22] Q. Xie, P. Chen, Phys. Rev. B 56 (1997) 5234.
[23] K.C. Mundim, L.A. Malbouisson, S. Dorfman, D. Fuks, J. Van Humbeek, V. Liubich, J. Mol. Struct. (Theochem) 539 (2001) 191.
[24] N. Juslin, P. Erhart, P. Träskelin, J. Nord, K.O. Enriksson, K. Nordlund, E. Salonen, K. Albe, J. Appl. Phys. 98 (2005) 123520.
[25] P.M. Derlet, D. Nguyen-Manh, S.L. Dudarev, Phys. Rev. B 76 (2007) 054107.
[26] M. Mrovec, R. Gröger, A.G. Bailey, D. Nguyen-Manh, C. Elsässer, V. Vitek, Phys. Rev. B 75 (2007) 104119.
[27] C. Domain, C.S. Becquart, Phys. Rev. B 65 (2001) 024103/1–024103/14.
[28] D.A. Terentyev, C. Lagerstedt, P. Olsson, K. Nordlund, J. Wallenius, C.S. Becquart, L. Malerba, J. Nucl. Mater. 351 (2006) 65.
[29] M.J. Attardo, J.M. Galligan, J.G.Y. Chow, Phys. Rev. Lett. 19 (1967) 73.
[30] J.A. DiCarlo, C.L. Snead, A.N. Goland, Phys. Rev. 178 (1969) 1059.
[31] S. Okuda, H. Mzubayashi, Phys. Rev. Lett. 34 (1975) 815.
[32] M.W. Guinan, R.M. Stuart, R.J. Borg, Phys. Rev. B 13 (1977) 699.
[33] M.H. Carlberg, E.P. Münger, L. Hultman, J. Phys.: Condens. Matter 12 (2000) 79.
[34] D. Nguyen Manh, A.P. Horsefield, S.L. Dudarev, Phys. Rev. B 73 (2006) 20101.
[35] C.S. Becquart, C. Domain, Nucl. Instrum. Meth. Phys. Res. B 255 (2007) 23.
[36] F. Dausinger, Philos. Mag. A 37 (1978) 819.
[37] R.R. Coltman, C.E. Klabunde, J.K. Redman, Phys. Rev. 156 (1967) 715.
[38] F. Maury, M. Biget, P. Vajda, A. Lucasson, P. Lucasson, Radiat. Effects 38 (1978) 53.
[39] J. Amano, D. Seidman, J. Appl. Phys. 56 (1984) 983.
[40] F. Dausinger, H. Schultz, Phys. Rev. Lett. 35 (1975) 1773.
[41] H. Tanimoto, M. Mzibayashi, H. Nishimura, S. Okuda, J. Phys. IV C8 (6) (1996) C8-285.
[42] S.L. Dudarev, C.R. Phys. 9 (2008) 409.
[43] J. Fikar, R. Schäublin, J. Nucl. Mater. 386–388 (2009) 97.
[44] H.J. Wollenberger, «Point defects» of «Physical Metallurgy», in: R.W. Cahn, P. Haasen (Eds.), third and enlarged ed., Elsevier Science Publisher BV, 1983 (Chapter 7).
[45] K. Maier, M. Peo, B. Saile, H.E. Schaefer, A. Seeger, Philos. Mag. A 40 (1979) 701.
[46] G. Neumann, V. Tölle, Philos. Mag. 61 (1990) 563.
[47] H. Mehrer, N. Stolica, N.A. Stolwijk, in: Landolt-Börnstein, H. Mehrer (Eds.), Data and Functional Relationships in Science and Technology, New Series III, vol. 26, Springer-Verlag, 1990, p. 48.
[48] C.C. Fu, Unpublished Results.
[49] R.W. Balluffi, J. Nucl. Mater. 69, 70 (1978) 240.
[50] J.N. Mundy, S.T. Ockers, L.C. Smedskjaer, Philos. Mag. A 56 (1987) 851.
[51] A. Satta, F. Willaime, S. de Gironcoli, Phys. Rev. B 57 (1998) 11184.
[52] J. Fikar, R. Schäublin, Nucl. Inst. Meth. Phys. Res. B 267 (2009) 3218.
[53] A.M. Guellil, J.B. Adams, J. Mater. Res. 7 (1992) 639.
[54] M.H. Carlberg, E.P. Münger, L. Hultman, J. Phys.: Condens. Matter 11 (1999) 6509.
[55] W.D. Wilson, R.A. Johnson, in: P.C. Gehlen, J.R. Beeler, R.I. Jaffee (Eds.), Interatomic Potentials and Simulation of Lattice Defects, Plenum, New York, 1972, p. 375.
[56] L.M. Caspers, H. van Dam, A. van Veen, Delft Progress Rep., Ser. A: Chem. Phys. Chem. Phys. Eng. 1 (1974) 39.
[57] A.A. Abrahamson, Phys. Rev. 130 (1963) 693.
[58] W.D. Wilson, C.L. Bisson, Radiat. Effects 22 (1974) 63.
[59] E.V. Kornelsen, Radiat. Effects 13 (1972) 227.
[60] D.E. Beck, Mol. Phys. 14 (1968) 311.
[61] K.O.E. Henriksson, K. Nordlind, J. Keinonen, D. Sundholm, M. Patzschkze, Phys. Scripta T108 (2004) 95.
[62] B. Delley, J. Chem. Phys. 92 (1990) 508. DMOL, Accelrys Inc., San Diego, US.
[63] A. van Veen, Mater. Sci. Forum Vol. 15–18 (1987) 3.
[64] C.S. Becquart, C. Domain, Phys. Rev. Lett. 97 (2006) 196402.
[65] C. Fu, F. Willaime, Phys. Rev. B 72 (2005) 064117.
[66] S.T. Picraux, F.L. Vook, Phys. Rev. Lett. 33 (1974) 1216.
[67] E. Ligeon, R. Danielou, J. Fontenille, R. Eymery, J. Appl. Phys. 59 (1986) 108.
[68] S. Nagata, K. Takahiro, J. Nucl. Mater. 283–2887 (2000) 1038.
[69] S.T. Picraux, F.L. Vook, J. Nucl. Mater. 53 (1974) 246.
[70] T. Seletskaia, Y. Osetsky, R. Stoller, G.M. Stocks, Phys. Rev. Lett. 94 (2005) 046403.
[71] N. Juslin, K. Nordlund, J. Nucl. Mater. 382 (2008) 143.
[72] N. Gao, M. Samaras, H. Van Swygenhoven, J. Nucl. Mater. 400 (2010) 240.
[73] T. Seletskaia, Yu.N. Osetsky, R.E. Stoller, G.M. Stocks, J. Nucl. Mater. 367–370 (2007) 355.
[74] A. Wagner, D.N. Seidman, Phys. Rev. Lett. 42 (1979) 515.
[75] G. Kresse, J. Hafner, Phys. Rev. B 47 (1993) 558;
Kresse, J. Hafner, Phys. Rev. B 49 (1994) 14251.
[76] G. Kresse, D. Joubert, Phys. Rev. B 59 (1999) 1758.
[77] J.P. Perdew, Y. Wang, Phys. Rev. B 45 (1991) 13244.
[78] H.J. Monkhorst, J.D. Pack, Phys. Rev. B 13 (1976) 5188.
[79] A.S. Soltan, R. Vassen, P. Jung, J. Appl. Phys. 70 (1991) 793.
[80] R.J.K. Nicholson, J.M. Walls, J. Nucl. Mater. 76,77 (1978) 251.
[81] H. Iwakiri, K. Yasunaga, K. Morishita, N. Yoshida, J. Nucl. Mater. 283–287 (2000) 1134.
[82] P. Jung, Private communication.
[83] K. Masuda, J. Phys. 43 (1982) 921.
[84] J.T. Buswell, Philos. Mag. 22 (1970) 787.
[85] J.T. Buswell, Philos. Mag. 22 (1970) 391.
[86] F. Häussermann, Philos. Mag. 25 (1972) 561.
[87] F. Häussermann, Philos. Mag. 25 (1972) 583.
[88] R.C. Rau, Philos. Mag. 18 (1970) 1079.
[89] D.N. Seidman, Surf. Sci. 70 (1978) 532.
[90] S. Takaki, J. Fuss, H. Kugler, U. Dedek, H. Schultz, Radiat. Effects 79 (1983) 87.
[91] A. Vehanen, P. Hautojarvi, J. Johansson, J. Yli-Kauppila, J.P. Moser, Phys. Rev. B 25 (1982) 762.
[92] D. Kato, Private communication.
[93] C.S. Becquart, C. Domain, J. Nucl. Mater. 385 (2009) 223.
[94] C.S. Becquart, J.M. Raulot, G. Bencteux, C. Domain, M. Perez, S. Garruchet, H. Nguyen, Comput. Mater. Sci. 40 (2007) 119.

[95] S.T. Picraux, J. Bøttiger, N. Rud, Appl. Phys. Lett. 28 (4) (1976) 179.
[96] S. Nagata, S. Yamamoto, K. Tokunaga, B. Tuschiya, K. Toh, T. Shikama, Nucl. Instrum. Methods, B 242 (2006) 553.
[97] J. Matolich, H. Nahm, J. Moteff, Scripta Met. 8 (1974) 837.
[98] R.K. Williams, F.W. Wiffen, J. Bentley, J.O. Stiegler, Metall. Trans. A 14 (1983) 655.
[99] R. Herschitz, D.N. Seidman, Acta Met. 32 (1984) 1141.
[100] Y. Nemoto, A. Hasegawa, M. Satou, K. Abe, J. Nucl. Mater. 283–287 (2000) 1144.